

# Operating Principles of Peristaltic Pumping through a Dense Array of Valves

Aaron Winn and Eleni Katifori

*Department of Physics and Astronomy, University of Pennsylvania, Philadelphia, PA 19104, USA*

Immersed nonlinear elements are prevalent in biological systems that require a preferential flow direction. A certain class of models is investigated where the fluid is driven by peristaltic pumping and the nonlinear elements are ideal valves that completely suppress backflow. This highly nonlinear system produces discontinuous solutions that are difficult to study. As the density of valves increases, the pressure and flow are well-approximated by a continuum of valves which can be analytically treated. Interestingly, two different pumping mechanisms emerge from this model. At low frequencies, diffusive transport pushes open all but one valve, and the radius takes the shape of the imposed force. At high frequencies, half of the valves open, and the flow is determined by the advective transport induced by peristalsis. In either case, the induced flow is linear in the amplitude of the peristaltic forces and is independent of pumping direction. Despite the continuum approximation used, the physical valve density is accounted for by modifying the resistance of the fluid appropriately. The suppression of backflow causes a net benefit in adding valves when the valve density is low, but once the density is high enough, the dominant valve effect is to suppress the forward flow, suggesting there is an optimum number of valves per wavelength.

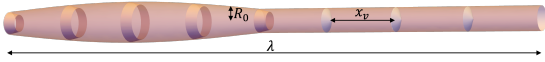


FIG. 1. Model for peristaltic pumping with many valves satisfying the assumption (1).

## I. INTRODUCTION

Peristalsis occurs when external radial forces propagate along a fluid-filled tube, inducing fluid motion. In the human body alone, peristaltic waves drive fluid transport in the esophagus [1], the ureter [2], the lymphatic system [3], and the perivascular spaces of the brain [4, 5]. The success of modeling peristaltic pumping arises from its simplicity. When only peristaltic forces drive flow and the forces take the form of a wave propagating in an infinitely long tube, the Navier Stokes equations describe steady flow in the co-moving wave frame. The problem of peristalsis at low Reynolds number was first studied perturbatively in powers of a small-amplitude parameter [6] and later extended to the case of arbitrary amplitudes, but under the assumption of long wavelength [7]. Historically, the term “long-wavelength peristalsis” has been used to refer to a regime where the wavelength is large compared to the (unperturbed) radius of the compliant tube  $R_0$ . When nonlinear elements are scattered throughout the tube, one has an additional length arising from the characteristic spacing between these elements. These nonlinear elements can be very important for determining the flow-pressure relationship of the tube, and as a result the function of the biological system they might describe, but introduce complexities that render an analytical treatment difficult. In this paper, we will consider the case when these nonlinear elements are valves that prevent backflow.

The combination of peristalsis and valves at low Reynolds

number is particularly relevant for studying biological fluid networks with a nonlinear pressure-flow relationship. For example, synchronous peristalsis in a finite tube capped with valves at both ends was used to model a bat wing venule [8]. Instead, here we would like to incorporate valves into a model for large-scale peristaltic pumping with many valves in an infinitely long tube. Our model closely resembles pumping in the collecting lymphatic vessels where intrinsic and extrinsic pumping mechanisms pump lymph through chains of lymphangions [3]. Throughout these larger vessels, the lymphatic system is a linear network with regularly spaced valves [9]. The peristaltic response in the lymphatic system is fundamentally different from that in the esophagus or the ureter in that the direction of fluid motion is fixed by the valve orientation, not the direction of peristaltic wave propagation. The fluid is transported in the valve direction even when the peristaltic wave travels in the opposite direction [10, 11]. Thus, unlike valveless peristalsis which is described by a vector quantity characterizing wave velocity, low-amplitude peristalsis with valves is largely described by a scalar quantity characterizing the frequency of oscillations.

In this paper, we will assume that the peristaltic wavelength  $\lambda$  is much longer than the characteristic valve spacing  $x_v$ .

$$R_0 \ll x_v \ll \lambda \quad (1)$$

The first inequality will allow us to neglect complicated behavior near the valves and apply the lubrication approximation. The second inequality will allow us to approximately recover wave-like behavior at large length scales. See figure 1 for an example geometry that satisfies approximation (1).

While focus will be given to this lymphatics-inspired model, the technique demonstrated in this paper could be used for a variety of problems containing a dense array of nonlinear elements satisfying (1), and could be of potential interest for engineering applications that incorporate artificial valves (see e.g. [12, 13]). This is the first paper to develop a method for treating peristalsis with many valves analytically. The key observation will be that the precise valve positions become unimportant when the valve density is large enough, and the flow is well-approximated by treating the entire tube as a valve.

This will be referred to as the valve continuum approximation. While a finite number of valves will break the symmetry required to study steady flow in the co-moving wave frame, this symmetry is restored in the valve continuum, allowing us to make analytical progress into this highly nonlinear problem.

The paper is outlined as follows. In section II, the fluid and solid mechanical equations governing force-imposed peristaltic pumping in a flexible tube are reviewed, along with the choice of non-dimensionalization. In section III, the equations for discrete ideal valves are introduced. It is then demonstrated how to coarse grain the fluid confined to regions of many closed valves in III A and many open valves in III B. From these considerations, one arrives at the model for a continuum of valves whose solutions are studied in section IV. Throughout this section, results will be presented for the case of a sinusoidal applied force. Discussion on how this model relates to the lymphatic system and additional applications will be given in section V. Additional mathematical details and results for a non-sinusoidal force will be given in the appendix.

## II. FORCE-IMPOSED PERISTALSIS AT LOW REYNOLDS NUMBER

There are two methods of mathematically modeling peristalsis on a cylindrical pipe. The most commonly used model assumes that the radius varies in time according to some prescribed function in the form of a wave  $R(x - vt)$ . This induces fluid motion in the tube, and the pressure and flow can be easily calculated [6, 7]. This method is appropriate for modeling the response from a peristaltic pump where the radius is fixed by the size of the rollers, but in the biological setting, it is more accurate to measure the fluid response from a force per area  $P_{\text{ext}}(x - vt)$  imposed on the pipe. This captures the fluid-structure interaction at the walls of the vessel. We will take the latter approach. We shall see that the former approach is compatible with the ideal valves studied here only in the limit of low-frequency peristaltic pumping. The goal of the paper will be to generalize the results of force-imposed peristalsis [14, 15] to the case with valves. In order to isolate the effects of peristalsis, the mean pressure drop per wavelength will be assumed zero throughout the paper.

### A. Dimensional Formulation

We will concern ourselves only with an incompressible fluid at low Reynolds number under the lubrication approximation. Since the radial velocity is always small, the pressure is only a function of the axial coordinate  $x$ , and the velocity profile remains parabolic. Thus, it is sufficient to work only in terms of the flow  $Q(x, t)$ , since the axial velocity  $u_x(x, r, t)$  can be recovered by using the following relations.

$$Q(x, t) \equiv \int_0^{R(x, t)} u_x(x, r, t) 2\pi r dr = \langle u_x \rangle (\pi R^2) \quad (2)$$

$$u_x(x, r, t) = 2\langle u_x \rangle \left[ 1 - \frac{r^2}{R^2} \right] \quad (3)$$

Here,  $R(x, t)$  is the radius of the tube. Under our approximations, the equations governing mass continuity and momentum conservation reduce to

$$\frac{\partial Q}{\partial x} + \pi \frac{\partial R^2}{\partial t} = 0 \quad (4)$$

$$\frac{\partial P}{\partial x} + \frac{8\mu}{\pi R^4} Q = 0. \quad (5)$$

Finally, we have a linear elasticity equation that couples the pressure to the radius. In general, this will involve terms that depend on the spatial derivatives of the radius, but at long wavelengths, the forces should be dominated by stretching of the form

$$P - P_{\text{ext}} = \frac{Eh}{(1 - \nu^2)R_0} \left( \frac{R}{R_0} - 1 \right) \quad (6)$$

where  $E$  is the Young's modulus,  $h$  is the thickness of the tube, and  $\nu$  is the Poisson's ratio [14, 16]. Consequences of adding a small bending term will be discussed in the appendix.  $P_{\text{ext}}$  is a periodic function with mean zero and characteristic amplitude  $P_a$ . Throughout most of the paper, we use  $P_{\text{ext}}(x, t) = P_a \cos(2\pi(x - vt)/\lambda)$  for numerical results, but the analytical results hold for any force that takes the form of a wave.

A table of symbols used throughout the paper is given in the appendix.

### B. Dimensionless Formulation

We will now work with convenient dimensionless quantities that make the frequency dependence of our functions most apparent.

$$\bar{R} \equiv \frac{R}{R_0}, \quad \bar{P} \equiv \frac{(1 - \nu^2)R_0}{Eh} P, \quad \bar{Q} \equiv \frac{8\mu}{\pi R_0^4} \frac{(1 - \nu^2)R_0\lambda}{Eh} Q, \quad f \equiv \frac{P_{\text{ext}}}{P_a} \quad (7)$$

$$\bar{x} \equiv \frac{x}{\lambda}, \quad \bar{t} \equiv \frac{\omega t}{2\pi} \quad (8)$$

$$\epsilon \equiv \frac{x_v}{\lambda}, \quad \omega\tau \equiv \omega \frac{4(1 - \nu^2)\mu\lambda^2}{\pi^2 E h R_0}, \quad \eta \equiv \frac{(1 - \nu^2)R_0}{Eh} P_a \quad (9)$$

Technically, the solutions will be a function of all of the valve positions  $\{x_v^i\}$ , but a particularly important quantity  $\epsilon$  is the ratio of the mean valve spacing  $x_v$  to the wavelength, which is small by (1). The two remaining parameters for our system,  $\eta$  and  $\omega\tau$ , can be thought of as competing effects between peristalsis and fluid flow in an elastic tube. The quantity  $\eta$  measures the strength of peristaltic forces relative to the stiffness of the tube.  $f$  is defined to be a dimensionless force that is presumably not much bigger than one. The quantity  $\omega\tau$  is the ratio of the elastic response time to the peristaltic period. Because the valves open and close with a period identical to the peristaltic period, the operation of the valves

changes drastically depending on whether the elastic tube has time to relax during one period. At small  $\eta$ , the pressure obeys a diffusion equation with diffusion constant  $\lambda^2/\tau$ . Thus, one can think of  $\omega\tau$  as a ratio of the peristaltic transport rate to the diffusive transport rate, much like the Péclet number used to describe transport of solutes in a fluid.

Using these dimensionless variables, our model for peristaltic pumping in an elastic tube becomes

$$\frac{\partial \bar{Q}}{\partial \bar{x}} + \pi\omega\tau \frac{\partial \bar{R}^2}{\partial \bar{t}} = 0 \quad (10)$$

$$\bar{Q} = -\bar{R}^4 \frac{\partial \bar{P}}{\partial \bar{x}} \quad (11)$$

$$\bar{P} - \eta f = \bar{R} - 1. \quad (12)$$

### III. INCORPORATING VALVES INTO A MODEL FOR PERISTALSIS

A valve could be any nonlinear element that promotes flow in one direction more than the other. We will concern ourselves only with the extreme case of a check valve, which only allows flow in one direction proportional to the pressure drop across the valve. This is equivalent to the diode representation of valves used in lumped models of the lymphatic system [9]. A more detailed valve model could incorporate the mechanical properties of the valves such as the bending and stretching stiffness [17]. Superscripts are used to index a particular valve; specifically,  $\bar{x}_v^i$  is used to denote the position of valve  $i$ , while  $\epsilon$  refers to the separation distance between valves in units of  $\lambda$ . We assume that the valve takes one of two states: open or closed. The status of the valve is determined by the sign of the pressure drop across the valve, such that the valve closes when the pressure downstream exceeds the pressure upstream, and the valve opens when the pressure upstream exceeds the pressure downstream. A closed valve has identically zero flow. An open valve has some finite pressure drop determined by Poiseuille's law.

Now, we'd like to treat these valves as zero dimensional elements coupled to a one-dimensional bulk. Denote the radial opening of the valve  $\bar{R}_v^i(\bar{x}, \bar{t})$ . This quantity should be proportional to the radius of the pipe where the valve is fixed  $\bar{R}(\bar{x}_v^i, \bar{t})$ . For any given open valve, assume that the occlusion fraction  $\sigma(\bar{x}) \equiv \bar{R}_v^i(\bar{x}, \bar{t})/\bar{R}(\bar{x}_v^i, \bar{t}) \in (0, 1]$  is independent of time or valve index. Then, we have a new dimensionless parameter that characterizes the resistance through any open valve of length  $\bar{b}$  in our system.

$$\bar{r}_v \equiv \int_{\bar{x}_v^i}^{\bar{x}_v^i + \bar{b}} \sigma(\bar{x})^{-4} d\bar{x} \quad (13)$$

More precisely,  $\bar{r}_v$  is the ratio of the fluidic resistance through an open valve to the fluidic resistance in a valveless tube of length  $\lambda$ . While any biological valve will break the rotation symmetry about the  $x$  axis assumed in this derivation and

illustrated in figure 1, one could still imagine assigning a valve resistance for any valve geometry by integrating the cross-sectional area through the leaflets. Assuming that the flow through the valve  $\bar{Q}_v^i(\bar{t})$  doesn't depend on the location in the valve, then  $\bar{Q}_v^i(\bar{t})$  is related to the pressure drop  $\Delta \bar{P}_v^i(\bar{t}) \equiv \bar{P}(\bar{x}_v^i, \bar{t}) - \bar{P}(\bar{x}_v^i + \bar{b}, \bar{t})$  by

$$\bar{Q}_v^i(\bar{t}) = \frac{\bar{R}(\bar{x}_v^i, \bar{t})^4}{\bar{r}_v} \Delta \bar{P}_v^i(\bar{t}) \Theta(\Delta \bar{P}_v^i(\bar{t})). \quad (14)$$

This equation governs the flow through our zero-dimensional valves. Incorporating these discrete elements into our fluid domain requires us to replace equation (11) by

$$\frac{\partial \bar{P}}{\partial \bar{x}} = -\bar{R}^{-4} \left[ 1 + \bar{r}_v \sum_i \delta(\bar{x} - \bar{x}_v^i) \Theta \left( - \frac{\partial \bar{P}}{\partial \bar{x}} \Big|_{\bar{x}_v^i} \right)^{-1} \right] \bar{Q}. \quad (15)$$

When the valve is open, there is a finite pressure drop over a small length scale  $\bar{b} \rightarrow 0$ . By integrating out the behavior near the valve, the pressure and radius will be discontinuous at each  $\{\bar{x}_v^i\}$  when  $\bar{r}_v \neq 0$ . It is worth emphasizing that when the Dirac delta function is integrated, the radius should be evaluated at the upstream radius (where the valve is anchored to the tube)  $\bar{R}(\bar{x}_v^i, \bar{t})$ .

Numerically, (15) is solved in conjunction with (10) and (12) over the domain  $(\bar{x}, \bar{t}) \in [0, 1] \times [0, 1]$  with periodic boundary conditions using a finite difference method for a given  $\eta$ ,  $\omega\tau$ ,  $\bar{r}_v$ , and  $\{\bar{x}_v^i\}$ . Valves are placed on a single edge in the spatial discretization, and the conductance is re-scaled appropriately at those edges. Care was taken to evaluate  $\bar{R}$  upstream when calculating the conductivity of an open valve. Solutions to these equations using  $f(\bar{x}, \bar{t}) = \cos(2\pi(\bar{x} - \bar{t}))$  are displayed in color in figure 2. To demonstrate the weak dependence on valve position, 20 valves were placed on the domain with mean spacing .05 and standard deviation .01. Regions of closed valves can be recognized by points where the flow is identically zero. Note that between two closely spaced valves, the flow is small when compared to the flow in regions with many open valves. The pressure has a characteristic step-like pattern in regions of closed valves. As the step size becomes smaller, the pressure seems to converge to a smooth curve proportional to  $f$ . The radius is the least well-behaved, showing large discontinuities at the locations of closed valves. The small jumps in  $\bar{P}$  and  $\bar{R}$  in the open sections are due to the finite open valve resistance. The goal of the next two sections will be to understand these cusps and discontinuities and find a way to smooth out the fluid dynamics in regions of open and closed valves that eliminates the explicit dependence on valve positions in (15). First, we will characterize  $\bar{P}$ ,  $\bar{Q}$ , and  $\bar{R}$  in powers of  $\epsilon$  in regions where valves are closed; in doing so, we will see that enforcing zero flow and a continuous pressure profile gives a good approximation to our collection of discretely placed closed valves. Then, we show how to coarse grain the resistance from many open valves. Throughout the rest of the paper, constant valve spacing will be assumed  $\bar{x}_v^i = i\epsilon$  for simplicity.

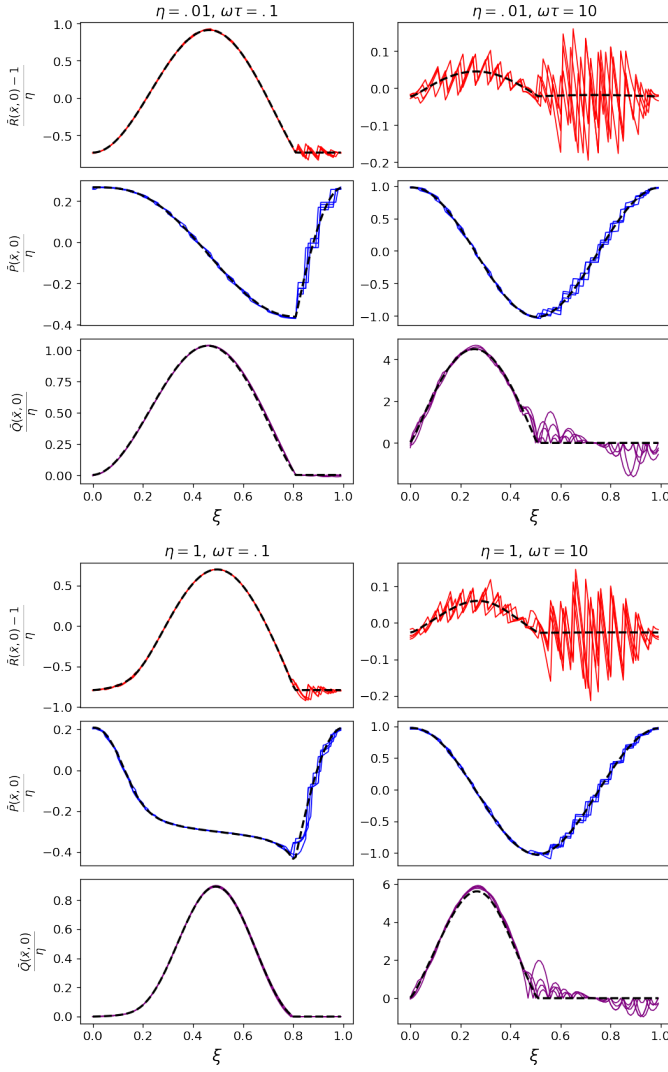


FIG. 2. Demonstration of how the pressure and flow in a system of many randomly placed valves is approximated by the results in the valve continuum limit. The colored solid lines show numerical results from simulating a tube with  $n_v = 20$  valves per wavelength. The dimensionless valve resistance was chosen to be  $\bar{r}_v = .02$ . The black dashed line shows the corresponding valve continuum prediction.

### A. Closely spaced valves suppress flow

The flow between two closed valves spaced a distance  $x_v$  apart is identically the flow in a flexible pipe of length  $x_v$  capped at both ends. When the valves are spaced much closer than  $\lambda$ , peristalsis is nearly synchronous across the entire pipe, and  $\epsilon$  can be used as an expansion parameter. We should change to using spatial coordinate  $\bar{y} \equiv \bar{x}/\epsilon$  such that the fluid between valves  $i$  and  $i+1$  is confined to an interval of length one,  $\bar{y} \in [\bar{y}_v^i, \bar{y}_v^{i+1}]$ . Since  $f$  is nearly constant in space between

two closed valves, we should Taylor expand  $f$  about  $\bar{x}_v^i$ .

$$f(\bar{y}, \bar{t}) = f(\bar{x}_v^i, \bar{t}) + \epsilon f'(\bar{x}_v^i, \bar{t})(\bar{y} - \bar{y}_v^i) + \epsilon^2 \frac{1}{2} f''(\bar{x}_v^i, \bar{t})(\bar{y} - \bar{y}_v^i)^2 + \dots$$

Here, the primes denote derivatives with respect to  $\bar{x}$ . Solving equations (10), (11), and (12) perturbatively with zero flow boundary conditions gives the following result.

$$\begin{aligned} \bar{P}^i(\bar{y}, \bar{t}) &= \bar{P}_0^i(\bar{t}) + \epsilon \bar{P}_1^i(\bar{t}) + \epsilon^2 \bar{P}_2^i(\bar{t}) + \epsilon^3 \bar{P}_3^i(\bar{y}, \bar{t}) + O(\epsilon^4) \\ &\approx \bar{R}_0 - 1 + \eta f(\bar{x}_v^i, \bar{t}) + \epsilon \left[ p_1 + \frac{1}{2} \eta f'(\bar{x}_v^i, \bar{t}) \right] \end{aligned}$$

$$\begin{aligned} \bar{Q}^i(\bar{y}, \bar{t}) &= \epsilon^2 \bar{Q}_2^i(\bar{y}, \bar{t}) + O(\epsilon^3) \\ &\approx -\epsilon^2 \pi \omega \tau \bar{R}_0 \eta f''(\bar{x}_v^i, \bar{t}) \left( (\bar{y} - \bar{y}_v^i)(\bar{y} - \bar{y}_v^{i+1}) \right) \end{aligned}$$

$$\begin{aligned} \bar{R}^i(\bar{y}, \bar{t}) &= \bar{R}_0 + \epsilon \bar{R}_1^i(\bar{y}, \bar{t}) + \epsilon^2 \bar{R}_2^i(\bar{y}, \bar{t}) + O(\epsilon^3) \\ &\approx \bar{R}_0 + \epsilon \left[ p_1 - \eta f'(\bar{x}_v^i, \bar{t}) \left( \bar{y} - \bar{y}_v^i - \frac{1}{2} \right) \right] \end{aligned}$$

Here,  $\bar{R}_0$  and  $p_1$  are undetermined constants whose value is unimportant at this stage of the analysis. The pressure is nearly constant in space, and the time dependence is fixed by the value of  $f(\bar{x}_v^i, \bar{t})$ . In fact, the  $\bar{y}$  dependence does not arise until  $O(\epsilon^3)$ , so the pressure between two closely spaced valves is nearly spatially independent, explaining the step-like profile observed in figure 2. The flow is everywhere continuous, but cusps can be seen at valves. There appears to be pockets of flow between two closed valves when  $\omega\tau$  is large. This is an immediate consequence of the continuity equation. The tube radius relaxes over a longer timescale when  $\omega\tau$  is large, so the fluid motion also persists longer. Crucially,  $\bar{Q}^i$  is suppressed by  $\epsilon^2$ , so the induced flow decreases rapidly as the volume of the storage region decreases. Although the  $O(\epsilon^0)$  term in  $\bar{R}$  is constant, the  $O(\epsilon^1)$  term has explicit  $\bar{y}$  dependence, arising from the slightly different forces applied across the length of the tube between two valves. This suggests that the approximation of constant radius will not be as good of an approximation as the approximations of constant pressure and zero flow as  $\epsilon$  approaches zero. The radial discontinuity across a valve located at  $\bar{x}_v^i$  is

$$\bar{R}^i(\bar{x}_v^i, \bar{t}) - \bar{R}^{i-1}(\bar{x}_v^i, \bar{t}) = \epsilon \eta f'(\bar{x}_v^i, \bar{t}). \quad (16)$$

This is exactly the change in radius from one side of the valve to the other  $\bar{R}^i(\bar{x}_v^i, \bar{t}) - \bar{R}^i(\bar{x}_v^{i+1}, \bar{t})$ . This explains why the radius rapidly oscillates between two values at order  $\epsilon$ , as observed in figure 2.

Continuous equations can be recovered by thinking of  $\bar{x}_v^i$  as a continuous variable and taking the limit  $\epsilon \rightarrow 0$ .

$$\bar{P}(\bar{x}, \bar{t}) \approx \bar{R}_0 - 1 + \eta f(\bar{x}, \bar{t}) + O(\epsilon) \quad (17)$$

$$\bar{Q}(\bar{x}, \bar{t}) \approx 0 + O(\epsilon^2) \quad (18)$$

$$\bar{R}(\bar{x}, \bar{t}) \approx \bar{R}_0 + O(\epsilon) \quad (19)$$

These equations will govern a dense region of closed valves. Although  $\bar{R} = \bar{R}_0$  does not seem to agree with the numerical solution, this will allow us to calculate the pressure and flow which do agree well with the numerical solution. It shouldn't be too surprising that the radius in the vicinity of closed valves is fixed to a constant value at leading order since any change in radius would induce flow which is prohibited. This is precisely why our valve model is inconsistent with radially imposed peristalsis. Having closed valves places a severe restriction on the types of allowed radial functions, so it doesn't make sense to impose  $\bar{R}$ . The model [8] utilizing ideal valves and radially imposed peristalsis considers the case of only two valves, and they find that at least one of the valves must be open at any time, avoiding the complication that arises when studying peristalsis between two closed valves. The one case where radially imposed peristalsis could work in our model is when  $\omega\tau$  is infinitesimal which we shall see corresponds to the special case of only one closed valve per wavelength.

### B. Flow through many open valves

Next, we seek a simplified model for a region with many open valves. The valves change the fluidic resistance over a small length scale, so we can apply the tools of homogenization theory to derive an appropriate effective resistance [18]. Our small dimensionless parameter will be  $\epsilon \equiv x_v/\lambda$  while the "fast" variable will be  $\bar{y} \equiv \bar{x}/\epsilon$ . We will expand each of our functions  $\bar{P}, \bar{Q}, \bar{R}$  in powers of  $\epsilon$ , and introduce  $n_v = \epsilon^{-1}$  which counts the number of valves per wavelength, with  $n_v \bar{r}_v \sim O(\epsilon^0)$ . In a region of open valves,

$$\left(\frac{\partial}{\partial \bar{x}} + \frac{1}{\epsilon} \frac{\partial}{\partial \bar{y}}\right) (\bar{Q}_0 + \epsilon \bar{Q}_1 + \dots) + \pi\omega\tau \frac{\partial}{\partial \bar{t}} (\bar{R}_0^2 + \dots) = 0. \quad (20)$$

$$\left(\frac{\partial}{\partial \bar{x}} + \frac{1}{\epsilon} \frac{\partial}{\partial \bar{y}}\right) (\bar{P}_0 + \epsilon \bar{P}_1 + \dots) = -(\bar{R}_0^{-4} + \dots) \left[1 + n_v \bar{r}_v \sum_i \delta(\bar{y} - \bar{y}_v^i)\right] (\bar{Q}_0 + \dots) \quad (21)$$

$$(\bar{P}_0 + \epsilon \bar{P}_1 + \dots) - \eta f = (\bar{R}_0 + \epsilon \bar{R}_1 + \dots) - 1 \quad (22)$$

From the  $O(\epsilon^{-1})$  terms in (20) and (21), we immediately learn that  $\bar{Q}_0$  and  $\bar{P}_0$  are independent of  $\bar{y}$ . From (22), we can also see that  $\bar{R}_0$  is independent of  $\bar{y}$ . At  $O(\epsilon^0)$  in equation (22), we have

$$\bar{P}_0 - \eta f = \bar{R}_0 - 1. \quad (23)$$

At  $O(\epsilon^0)$  in equation (20), we have

$$\frac{\partial \bar{Q}_0}{\partial \bar{x}} + \frac{\partial \bar{Q}_1}{\partial \bar{y}} + \pi\omega\tau \frac{\partial \bar{R}_0^2}{\partial \bar{t}} = 0.$$

Since  $\bar{y}$  is periodic, we can integrate  $\bar{y}$  over the unit interval to obtain

$$\frac{\partial \bar{Q}_0}{\partial \bar{x}} + \pi\omega\tau \frac{\partial \bar{R}_0^2}{\partial \bar{t}} = 0 \quad (24)$$

which enforces

$$\frac{\partial \bar{Q}_1}{\partial \bar{y}} = 0.$$

Looking at  $O(\epsilon^0)$  in equation (21),

$$\frac{\partial \bar{P}_0}{\partial \bar{x}} + \frac{\partial \bar{P}_1}{\partial \bar{y}} = -\bar{R}_0^{-4} \left[1 + n_v \bar{r}_v \sum_i \delta(\bar{y} - \bar{y}_v^i)\right] \bar{Q}_0.$$

Integrating  $\bar{y}$  over the unit interval gives

$$\frac{\partial \bar{P}_0}{\partial \bar{x}} = -\bar{R}_0^{-4} \left[1 + n_v \bar{r}_v\right] \bar{Q}_0. \quad (25)$$

This along with (22) requires

$$\frac{\partial \bar{P}_1}{\partial \bar{y}} = -n_v \bar{r}_v \bar{R}_0^{-4} \left[\sum_i \delta(\bar{y} - \bar{y}_v^i) - 1\right] \bar{Q}_0 = \frac{\partial \bar{R}_1}{\partial \bar{y}}.$$

It is now clear that a region of open valves is described using the continuity (23) and force-balance (24) equations for a valveless pipe, but with a modified momentum equation (25) that takes into account the coarse-grained valve resistance. This equation could have been guessed by adding the resistance of our tube and  $n_v$  valves in series. The differential equations (23), (24), and (25) are written entirely in terms of the continuous functions  $\bar{P}_0, \bar{Q}_0$ , and  $\bar{R}_0$ . While  $\bar{P}_1$  and  $\bar{R}_1$  are both discontinuous at the valves (and contain identical  $\bar{y}$  dependence),  $\bar{Q}_1$  is independent of the microscopic coordinate  $\bar{y}$ , so much like the theory for regions of closed valves, the leading-order term in our expansion for regions of open valves works particularly well at describing the flow which is the fundamental quantity of interest.

The dependence on valve parameters can be eliminated by defining new dimensionless quantities.

$$\bar{\bar{Q}}_0 \equiv \left[1 + n_v \bar{r}_v\right] \bar{Q}_0, \quad \omega \bar{\tau} \equiv \omega \left[1 + n_v \bar{r}_v\right] \tau$$

The culmination of this section is a complete description of the fluid in a dense array of valves in terms of the continuous functions  $\bar{\bar{P}}_0, \bar{\bar{R}}_0$ , and  $\bar{\bar{Q}}_0$  and two dimensionless parameters  $\eta$  and  $\omega \bar{\tau}$ , which is the same number of parameters needed for the valveless problem. Throughout the next section, all analytical results are presented in the limit  $\epsilon \rightarrow 0$ , and the subscript zero will be re-purposed for a new perturbative expansion.

## IV. VALVE CONTINUUM

Combining the results of the previous two sections gives us the behavior of  $\bar{\bar{P}}, \bar{\bar{Q}}$ , and  $\bar{\bar{R}}$  when  $\epsilon \rightarrow 0$ . The motivation for studying this regime of dense valves is that we have

eliminated any dependence on the valve positions  $\{\bar{x}_v^i\}$  and by appropriate rescaling have even eliminated  $\bar{r}_v$ , leaving only two parameters characterizing the peristaltic pumping. The only spatial dependence remaining comes from the peristaltic force  $f$ . Because we are assuming  $f$  takes the form of a wave, we seek wave solutions in terms of the coordinate  $\xi \equiv \bar{x} - \bar{t}$ . As a matter of personal preference, solutions are given in the lab frame, so no additional coordinate transformation of  $\bar{Q}$  is necessary. For simplicity, it is assumed that the wave always travels in the same direction as the valves are oriented.

$$\frac{d}{d\xi} \left[ \bar{Q} - \pi\omega\bar{\tau}\bar{R}^2 \right] = 0 \quad (26)$$

$$\bar{Q} = -\bar{R}^4 \frac{d\bar{P}}{d\xi} \Theta \left( -\frac{d\bar{P}}{d\xi} \right) \quad (27)$$

$$\bar{P} - \eta f = \bar{R} - 1 \quad (28)$$

In figure 2, example solutions to (26), (27), and (28) are shown as black dashed lines and compared to that predicted by (10), (12), and (15) in color. Note that for the flow, it is the quantity  $\bar{Q}$  that is plotted even for the valve continuum case, so once  $\bar{Q}$  is obtained using the above equations, one must divide by  $1 + n_v \bar{r}_v$  in order to see agreement with the discrete valve model.

This system can be solved analytically by splitting into regions of open and closed valves, denoted with superscripts  $O$  and  $C$  respectively. When the valves are closed, we can use the solutions from section III A.

$$\bar{Q}^C(\xi) = 0 \quad (29)$$

$$\bar{P}^C(\xi) = \bar{R}^C - 1 + \eta f(\xi) \quad (30)$$

$$\bar{R}^C(\xi) = \bar{R}^C \quad (31)$$

In order to fix  $\bar{R}^C$ , we impose that the mean area is identically 1.

$$\langle \bar{R}^2 \rangle \equiv \int_0^1 d\xi \bar{R}^2(\xi) = 1. \quad (32)$$

For the open valve problem, we can first decouple our equations and solve a differential equation for  $\bar{R}$ . Define  $\xi = 0$  to be the location where the valves transition from closed to open such that  $\bar{R}^O(0) = \bar{R}^C$ . This gives us a single nonlinear ODE in  $\bar{R}^O$

$$\frac{d\bar{R}^O}{d\xi} = -\pi\omega\bar{\tau}(\bar{R}^O)^{-4} \left( (\bar{R}^O)^2 - (\bar{R}^C)^2 \right) - \eta \frac{df}{d\xi} \quad (33)$$

that can be solved perturbatively by writing  $\bar{R}^O(\xi) = 1 + \sum_{n=1}^{\infty} \eta^n \bar{R}_n^O(\xi)$  and  $\bar{R}^C = 1 + \sum_{n=1}^{\infty} \eta^n \bar{R}_n^C$ . Similar notation is used to expand the pressure and flow in powers of  $\eta$ . Note that the same notation was used in the previous section for a perturbative expansion in  $\epsilon$ , but throughout the rest of the paper, numerical subscripts refer to terms in a perturbative expansion in  $\eta$ .

### A. Small amplitude peristalsis

Now, we attempt to solve equation (33) up to order  $\eta$ .

$$\frac{d\bar{R}_1^O}{d\xi} = -2\pi\omega\bar{\tau}(\bar{R}_1^O - \bar{R}_1^C) - \frac{df}{d\xi} \quad (34)$$

Let  $\tilde{\xi}$  denote the coordinate at which the valves close, and let  $\tilde{\xi}_1$  denote the coordinate at which the valves close assuming  $\bar{R} = \bar{R}_1$ . Then our boundary conditions are  $\bar{R}_1^O(0) = \bar{R}_1^C$  and  $\bar{R}_1^O(\tilde{\xi}_1) = \bar{R}_1^C$ . The solution to this differential equation is

$$\bar{R}_1^O(\xi) = \bar{R}_1^C - \int_0^\xi d\xi' \frac{df}{d\xi'} e^{2\pi\omega\bar{\tau}(\xi' - \xi)} \quad (35)$$

where  $\tilde{\xi}_1$  satisfies

$$\int_0^{\tilde{\xi}_1} d\xi' \frac{df(\xi')}{d\xi'} e^{2\pi\omega\bar{\tau}(\xi' - \tilde{\xi}_1)} = 0. \quad (36)$$

There could potentially be many opening and closing events, but when  $f$  is a sine wave or a Gaussian wave train, there is only a single solution for  $\tilde{\xi}_1 \in (0, 1]$ . Since  $f$  is a periodic function, it is also useful to write this equation in terms of the Fourier transform of  $f$ ,  $f = \sum_m f_m e^{2\pi i m \xi}$ .

$$\sum_m f_m \frac{im}{\omega\tau + im} \left[ e^{2\pi i m \tilde{\xi}_1} - e^{-2\pi\omega\bar{\tau}\tilde{\xi}_1} \right] = 0 \quad (37)$$

Imposing the area constraint (32) fixes  $\bar{R}_1^C$ .

$$\begin{aligned} 0 &= \int_0^1 \bar{R}_1 d\xi = \bar{R}_1^C - \sum_m f_m \frac{im}{\omega\tau + im} \left[ \frac{e^{2\pi i m \tilde{\xi}_1} - 1}{2\pi i m} + \frac{e^{-2\pi\omega\bar{\tau}\tilde{\xi}_1} - 1}{2\pi\omega\bar{\tau}} \right] \\ &= \bar{R}_1^C - \frac{1}{2\pi\omega\bar{\tau}} \sum_m f_m [e^{2\pi i m \tilde{\xi}_1} - 1] = \bar{R}_1^C - \frac{1}{2\pi\omega\bar{\tau}} [f(\tilde{\xi}_1) - f(0)] \end{aligned}$$

We now have  $\bar{R}_1$  and can easily write down  $\bar{R}$ ,  $\bar{P}$ , and  $\bar{Q}$  up to order  $\eta$ .

$$\bar{R}(\xi) = \begin{cases} 1 - \frac{\eta}{2\pi\omega\bar{\tau}} [f(0) - f(\tilde{\xi})] - \eta \int_0^\xi d\xi' \frac{df}{d\xi'} e^{2\pi\omega\bar{\tau}(\xi' - \xi)}, & \text{for } 0 \leq \xi \leq \tilde{\xi} \\ 1 - \frac{\eta}{2\pi\omega\bar{\tau}} [f(0) - f(\tilde{\xi})], & \text{for } \tilde{\xi} \leq \xi \leq 1 \end{cases} \quad (38)$$

$$\bar{P}(\xi) = \begin{cases} \eta f(\xi) - \frac{\eta [f(0) - f(\tilde{\xi})]}{2\pi\omega\bar{\tau}} - \eta \int_0^\xi d\xi' \frac{df}{d\xi'} e^{2\pi\omega\bar{\tau}(\xi' - \xi)}, & \text{for } 0 \leq \xi \leq \tilde{\xi} \\ \eta f(\xi) - \frac{\eta [f(0) - f(\tilde{\xi})]}{2\pi\omega\bar{\tau}}, & \text{for } \tilde{\xi} \leq \xi \leq 1 \end{cases} \quad (39)$$

$$\bar{Q}(\xi) = \begin{cases} -2\pi\omega\bar{\tau}\eta \int_0^\xi d\xi' \frac{df}{d\xi'} e^{2\pi\omega\bar{\tau}(\xi' - \xi)}, & \text{for } 0 \leq \xi \leq \tilde{\xi} \\ 0, & \text{for } \tilde{\xi} \leq \xi \leq 1 \end{cases} \quad (40)$$

When  $\omega\bar{\tau}$  is small, the diffusion constant is large, causing the force to spread throughout the channel. The valves prevent

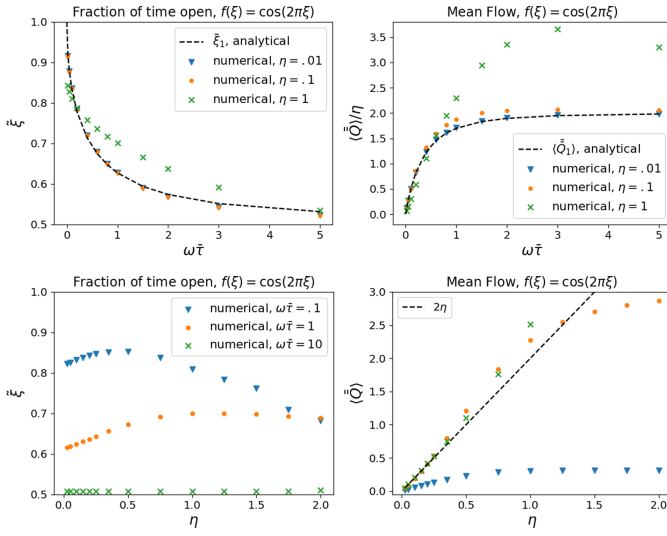


FIG. 3. Results for the valve continuum model when driven with a sinusoidal external force. Numerical simulations were performed for various choices of  $\eta$  and  $\omega\bar{\tau}$ . The dashed lines represent the analytic results given in equations (36) and (41), respectively.

diffusion in the reverse direction, so peristalsis with a small  $\omega\bar{\tau}$  has a tendency to push a pressure wave forward over a longer range than the case for large  $\omega\bar{\tau}$ . The radial function then expands over the full region of open valves. At low frequencies, the radius has more time to expand as the wave passes, so the magnitude of  $\bar{R} - 1$  is larger for smaller  $\omega\bar{\tau}$ . The pumping strategies for the small and large  $\omega\bar{\tau}$  cases are qualitatively different. At low frequencies, the valves are nearly all open, but only small amounts of flow diffuse through the system. At higher frequencies, about half of the valves are open, and a large volume of fluid is transported through the open valves by the action of peristalsis.

Additionally, we can calculate the mean flow in terms of  $\tilde{\xi}_1$ .

$$\langle \bar{Q}_1 \rangle = 2\pi\omega\bar{\tau} \int_0^1 (\bar{R}_1 - \bar{R}_1^C) d\xi' = f(0) - f(\tilde{\xi}_1) \quad (41)$$

Of course, evaluating this simple-looking equation requires knowing  $\tilde{\xi}_1$  which depends on  $\omega\bar{\tau}$ . Two cases can be solved exactly: When  $\omega\bar{\tau} \rightarrow 0$ ,  $\tilde{\xi}_1 = 1$ , and  $\langle \bar{Q}_1 \rangle \rightarrow 0$ ; when  $\omega\bar{\tau} \rightarrow \infty$ ,  $f'(\tilde{\xi}_1) = 0$ . For example, if  $f(\xi) = \cos(2\pi\xi)$ , then the maximum flow at a high frequency is 2. Note that  $\tilde{\xi}$  can also be interpreted as the fraction of time a valve is open. That is, a valve is almost always open when  $\omega\bar{\tau}$  is small, while it is only open half the time when  $\omega\bar{\tau}$  is large. These results are displayed in figure 3. When  $\omega\bar{\tau}$  is small, the forward diffusion mechanism pushes open nearly all the valves (all but one which single-handedly prevents any backflow). At larger values of  $\omega\bar{\tau}$ , the pressure is largely determined by  $f$ , which for the case of a cosine wave has positive slope half the time and negative slope half the time. For intermediate values of  $\omega\bar{\tau}$ ,  $\tilde{\xi}$  can be understood as a combination of these diffusion-driven and external-force-driven mechanisms.  $\langle \bar{Q}_1 \rangle$  is necessarily zero when the frequency vanishes since there is

no peristalsis in this case, and it increases monotonically with frequency. Compare this result to the valveless problem where mean flow vanishes at order  $\eta$ , and so the leading-order flow response to peristalsis is characterized by  $\langle \bar{Q}_2 \rangle$  [14]. For the valveless case, the fluid is pushed by the action of peristalsis, but for the case with valves, the oscillatory flow induced at order  $\eta$  is rectified by the valves, giving a nonzero  $\langle \bar{Q}_1 \rangle$ .

## B. Large amplitude peristalsis

It is deceptively difficult to continue our analysis to higher order in  $\eta$  analytically due to the challenge in finding higher-order corrections to  $\tilde{\xi}$ , so even for moderate-amplitude peristalsis, one must resort to numerically solving (26), (27), and (28). Although the response to the applied force becomes highly nonlinear, we still see that larger forces cause larger deformations. The normalized tube radius becomes much less than one at certain locations and much larger than 1 at others. For moderate  $\eta$ , the mean flow increases faster than linear in  $\eta$ , which is not surprising since open valves act much like a valveless pipe where the mean flow grows as  $\eta^2$ .

## C. Valve density

One enlightening application of this model is to estimate the density of valves that optimizes the mean flow (see e.g. [19]). The valves introduce competing effects. Some valves are necessary to prevent backflow, but for  $\bar{r}_v \neq 0$ , an excessive number of valves will increase the fluidic resistance and thus lower the magnitude of the flow. See figure 4. When  $\bar{r}_v = 0$ , the flow increases monotonically with  $n_v$ , eventually reaching an asymptote given by the valve continuum model. When  $\eta$  is large, the flow is dominated by valveless peristalsis at order  $\eta^2$ , so having few or no valves is optimal. The interesting case is when  $\eta$  is small and  $\bar{r}_v \neq 0$ . Here, we see that there is a finite optimum number of valves that maximizes the mean flow which will be denoted  $n_v^*$ . At small  $n_v$ , the dominant valve effect is to prevent backflow, but at large  $n_v$ , the valve continuum model predicts a decay in the mean flow

$$\langle \bar{Q}_1 \rangle = \frac{\langle \bar{Q}_1 \rangle}{1 + \bar{r}_v n_v} = \frac{[f(0) - f(\tilde{\xi}_1)]}{1 + \bar{r}_v n_v}. \quad (42)$$

In figure 5, the optimum number of valves  $n_v^*$  is plotted against  $\bar{r}_v$  for several different choices of  $\omega\tau$  and  $\eta$  on a log-log scale. To obtain each data point in this plot, the mean flow is calculated for a particular  $\omega\tau$ ,  $\eta$ , and  $\bar{r}_v$  while  $n_v$  is varied from zero up to 36 (where the valve continuum model certainly holds) in integer steps. The sudden dropoff at large  $\bar{r}_v$  occurs when the optimum number of valves (for all  $n_v$  tested) is zero. Note that  $n_v$  can be made fractional by extending the computational domain over several wavelengths. In order to study the case of  $p/q$  valves per wavelength where  $p$  and  $q$  are positive integers, one would place  $p$  valves on a domain of length  $q$ . This could be used to study systems with low valve density which is the

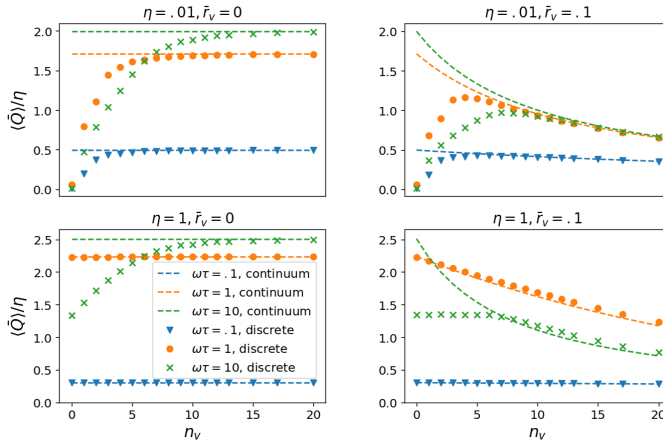


FIG. 4. Mean flow as a function of the number of valves per wavelength  $n_v = \epsilon^{-1}$ . As the density increases, the mean flow approaches the valve continuum result and eventually scales according to equation (42).

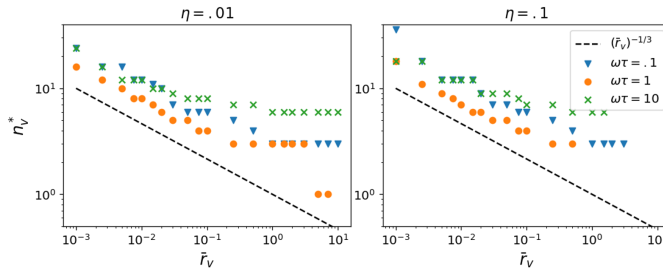


FIG. 5. Optimum number of valves per wavelength  $n_v^*$  as a function of the dimensionless valve resistance  $\bar{r}_v$

opposite limit studied in this paper. For  $\bar{r}_v \ll 1$ , it is beneficial to have multiple valves per wavelength, and the optimum number seems to scale as a power law in  $\bar{r}_v$ .

## V. DISCUSSION

### A. Application: Lymphatic system

In order to apply the results of this paper to the lymphatic system, we must first check that our models for the fluid, vessel, and valve are appropriate. If so, then we may check that approximation (1) holds and study the implications of our valve continuum model.

Lymph can be treated at zero Reynolds number when the diameters are less than  $100 \mu\text{m}$  [3]. This is the case for the rat mesenteric lymphatics, where the Reynolds number was experimentally calculated to be  $.045$  [20]. However, in the largest lymphatic vessel in the human body, the thoracic duct, the diameters are closer to  $2 \text{ mm}$ , and the flow is laminar.

It is widely accepted in the lymphatics literature that the valves operate via the pressure drop across the valve. It was shown that the aspect ratio of lymphatic valves (what we call

$b/2R_0$ ) is above a critical threshold that allows for complete closure of the valves under adverse pressure conditions [21]. It is also noted that an open valve contributes a resistance comparable to the vessel in some cases. Further details of lymphatic valves including valve stiffness [21] and hysteretic pressure response [22] have been incorporated into computational models.

Experimental data on lymphatic pumping is plentiful, but few studies have been able to resolve the propagation of peristaltic waves. When only a single lymphangion is studied, the whole vessel appears to contract uniformly [3]. Thus, the ratio  $x_v/\lambda$  is difficult to find in the literature, while  $R_0/x_v$  can be found in numerous sources. A detailed study of the peristaltic waves in mesenteric rat lymphatics is given in [11]. The authors demonstrate that 80-90 percent of waves are coordinated, meaning contractions are observed in adjacent sites within one second of each other. The waves were observed to propagate at a speed of  $6 \pm 2 \text{ mm/s}$  at a contraction frequency of  $.0875 \pm .01/\text{s}$ . The calculated wavelength is  $\lambda = 69 \pm 24 \text{ mm}$ , consistent with nearly synchronous oscillations on length scales comparable to the size of the rat. The radii of these vessels was measured to be  $R_0 = .045 \pm .015 \text{ mm}$ , and  $x_v = .8 \pm .2 \text{ mm}$ . Thus, we can safely say  $R_0 \ll x_v \ll \lambda$ . For bovine mesenteric lymphatics, the contraction waves were seen to propagate at  $4\text{-}5 \text{ mm/s}$  with a frequency of  $4\text{-}6/\text{min}$ , indicating a wavelength of  $\lambda = 54 \pm 12 \text{ mm}$  [23]. However, the radii of these vessels was much larger,  $R_0 = .25\text{--}1.5 \text{ mm}$ , with a valve spacing closer to  $20 \text{ mm}$  [24]. For these larger vessels, the discrete nature of the valves may be important.

Estimating  $\omega\tau$  is also challenging. Intrinsic contractions in the lymphatic system are often modeled using a time-varying elastance, so  $E$  cannot be thought of as constant. Macdonald considers a range of values between  $1250$  and  $7500 \text{ Pa}$  when modeling bovine lymphatics [24]. The thickness  $h$  is generally considered to be proportional to the radius ( $h/R_0 \approx .1$ ). Since the radius changes so much between different vessels, it is useful to write

$$\tau = \left[ \frac{4(1-\nu^2)\mu}{\pi^2 E(h/R_0)} \right] \left( \frac{\lambda}{R_0} \right)^2 \equiv \tau_0 \left( \frac{\lambda}{R_0} \right)^2. \quad (43)$$

With the error dominated by the range of  $E$  values, we can estimate  $\tau_0 = 3.6 \times 10^{-7} - 2.2 \times 10^{-6} \text{ s}$ . Using the length scales for the rat mesentery,  $(\lambda/R_0)^2 = 5.6 \times 10^5 - 9.6 \times 10^6$ , leading to a relaxation time of  $\tau = .20 - 21 \text{ s}$ . For the bovine mesentery,  $(\lambda/R_0)^2 = 7.8 \times 10^2 - 7.0 \times 10^4$ , leading to a relaxation time of  $\tau = .00028 - .15 \text{ s}$ . Incorporating the known frequencies leads to estimates of  $\omega\tau = .1 - 10$  for the rat and  $\omega\tau = 10^{-4} - .1$ . The variation in Young's modulus and radius along with the uncertainty in the wavelength suggests that a wide range of  $\omega\tau$  values should be studied, as we have in this paper.

The exact value of  $\eta$  is unimportant, but it is reasonable to assume that the lymphatic system operates in the regime of small-amplitude peristalsis. Experimentally, one can see that the radius changes by no more than one third of its rest value [11]. If the lymphatic system operated in a regime of large-amplitude peristalsis, then valves would be unnecessary since the peristalsis could push the fluid without valves.



Physical parameter	Measured Value	Reference
Viscosity $\mu$	$8.9 \times 10^{-4}$ Pa $\cdot$ s	[24]
Poisson ratio $\nu$	.5	[24]
Young's modulus $E$	1250 - 7500 Pa	[24]
Tube thickness $h/R_0$	.036 - .1	[24]
Rest radius $R_0$ (rat)	.03 - .06 mm	[11]
Rest radius $R_0$ (bovine)	.25 - 1.5 mm	[11]
Valve spacing $x_v$ (rat)	.6 - 1.0 mm	[11]
Valve spacing $x_v$ (bovine)	$\approx 20$ mm	[24]
Wavelength $\lambda$ (rat)	$69 \pm 24$ mm	calculated from [11]
Wavelength $\lambda$ (bovine)	$54 \pm 12$ mm	calculated from [24]
Contraction frequency $\frac{\omega}{2\pi}$	.067 - .10 s $^{-1}$	[11], [24]
$\omega\tau$	$10^{-5}$ - 10	calculated
$\eta$	< 1	[11]
$\bar{r}_v$	.07 $\pm$ .02	calculated from [25]

TABLE I. Experimental values of physical parameters in the lymphatic system.

It is slightly easier to estimate the valve resistance  $\bar{r}_v$ . The length of the valve  $b$  is going to be larger than but on the order of  $R_0$  to ensure valve closure. Confocal microscopy has been used to carefully examine the valves in the rat mesentery [25]. They found  $b \approx 3R_0$  and the outlet cross-sectional area is one sixth the inlet cross-sectional area. Naively treating the entire valve as having  $\sigma = 1/\sqrt{6}$  leads to an overestimate of the valve resistance of  $\bar{r}_v = .07$ . More carefully integrating over the valve, assuming a square root function describes the valve shape, gives a value closer to  $\bar{r}_v = .05$ . In either case, this puts us in the regime where having more than tens of valves per wavelength would lead to an excessive amount of valve resistance, reducing the flow in the forward direction. The predicted optimum number of valves for this valve resistance is between five and ten, depending on the exact value of  $\omega\tau$ . This is about one order of magnitude smaller than the experimental value.

All of these considerations suggest that we should be able to at least qualitatively apply the small-amplitude valve continuum results to the lymphatic system.

## B. Summary

In this paper, we showed that a two-state immersed nonlinear element can be modeled using continuous differential equations by splitting into two regions. When considered in small numbers, the valves produce discontinuous pressure profiles and do not support wave-like solutions typical of peristaltic pumping. Interestingly, we recovered both a continuous pressure profile and wave solutions by considering the limit of an infinite density of valves. One may naively think that the solutions to these equations can be obtained by solving the valveless model and setting all negative-flow regions to have identically zero flow. This is not the case. In fact, this under-

estimates the mean flow for our problem. This intuition holds true when  $\omega\tau$  is large; in this case, the pressure profile closely resembles the external pressure, and the fluid is driven by the components of peristalsis that lower the pressure downstream while the valves prevent backflow when the pressure is lower upstream. However, when  $\omega\tau$  is small, there is an additional diffusion mechanism that needs to be considered. Since the period of the peristaltic wave is longer than the relaxation time of the vessel, the tube relaxes and the fluid diffuses, but with a bias for the forward direction. The interaction between the fluid, tube, and valves could only be taken into account by imposing a force on the tube as opposed to the traditional method of imposing a radial function. Approaching the valve continuum, the flow increases with valve density as more oscillations are rectified, but the presence of a nonzero valve resistance reduces the flow causing a decay in the mean flow proportional to  $n_v^{-1}$ .

Since systems containing lower-dimensional nonlinear elements arise throughout biology, care must be taken to predict the effective flow properties. One must first determine how the fluid behaves between the individual elements. From this, one can write down simpler equations describing the large-scale flow, analogous to the models used for peristalsis without valves. Similar approaches have been used to characterize the effective resistance around soft hair beds [26], brushes, and carpets [27]. This is the first paper to derive the coarse-grained behavior for a system consisting of many ideal valves without appealing to lumped-parameter modeling. We believe the steps taken in this paper could guide future works related to pumping around similar highly nonlinear elements. Finally, the simplifications made in this paper will allow for the study of biologically inspired nonlinear fluidic networks without explicit dependence on the valve positions. This topic will be explored in future work.

## Appendix A

### 1. Elaborating on the radial discontinuity

A surprising consequence of using ideal valves is the presence of a spatial discontinuity in the radial function  $\bar{R}$  and a cusp in  $\bar{Q}$ . Physically, this result seems counterintuitive. Even when the fluid is confined to a small space, the side that experiences a greater inward force will contract while the other side will expand. Within a single lymphangion, this seems like a reasonable conclusion, and since our force balance equation (12) only accounts for radial forces, there is no coupling between two adjacent lymphangions. To solve this problem, we can add a small bending force so that our force-balance equation becomes

$$P - P_{\text{ext}} = \frac{Eh}{(1 - \nu^2)R_0} \left[ h^2 R_0^2 \frac{\partial^4}{\partial x^4} \left( \frac{R}{R_0} - 1 \right) + \left( \frac{R}{R_0} - 1 \right) \right]. \quad (\text{A1})$$

Alternatively, any other force that depends on the spatial derivatives of  $R$  (such as tension) should resolve our problem [24]. Since  $h^2 R_0^2 / \lambda^4 \ll 1$ , it is tempting to drop the bending

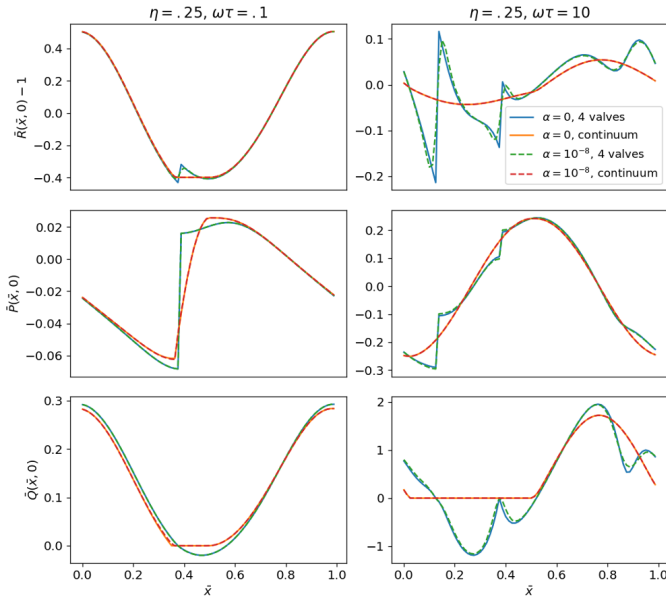


FIG. 6. A comparison between the results with and without a small bending term in equation (A1). Here  $\alpha \equiv h^2 R_0^2 / \lambda^4$  is a dimensionless parameter characterizing the strength of bend.

terms and focus only on the stretching as we did throughout the paper. Indeed, this new term does not affect the large scale pumping properties in the tube, justifying our use of (12). See figure 6. The solutions with and without bend for a realistic choice of  $\alpha \equiv h^2 R_0^2 / \lambda^4$  differ only near the closed valves. Introducing a small bending term smooths out  $\bar{R}$  and  $\bar{Q}$ , but the pressure distribution is kept discontinuous. The mean flow for the two cases is essentially the same. Notice that approximation (1) guarantees any force dependent on spatial derivatives of  $R$  will be small.

## 2. Gaussian forcing

In the main text, all results were given assuming  $f(\xi) = \cos(2\pi\xi)$ . In order to demonstrate the generality of our small

amplitude results, here we show the results when  $f$  takes the form of a Gaussian wave train.

$$f(\xi) = \frac{1}{\sqrt{2\pi}a^2} \sum_{m \in \mathbb{Z}} e^{-\frac{(\xi-m)^2}{2a^2}} - 1 \quad (\text{A2})$$

Notice that  $f'(0) = 0$ , and  $f''(0) < 0$  so that the valve opens at  $\xi = 0$ . A summary of the results with a comparison to the theory is given in figure 7. The small-amplitude theory works well at approximating the fraction of open valves and mean flow when  $\eta < 1$ , just like with the sinusoidal forcing.

## 3. Table of parameters

See II for a summary of parameters used in the paper.

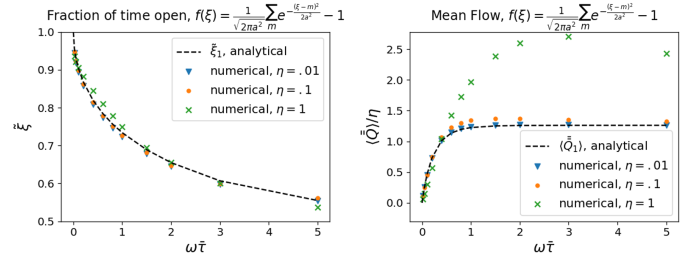


FIG. 7. Summary of results for a Gaussian forcing with width parameter  $a = .1$ .

## ACKNOWLEDGMENTS

The authors thank Yoichiro Mori for helpful discussions. This research was supported by the NSF Award PHY-1554887, the University of Pennsylvania Materials Research Science and Engineering Center (MRSEC) through Award DMR-1720530, and the Simons Foundation through Award 568888.

- 
- [1] J. G. Brasseur, *Dysphagia* **2**, 32 (1987).
  - [2] E. O. Carew and T. J. Pedley, *Journal of Biomechanical Engineering* **119**, 66 (1997).
  - [3] J. E. Moore and C. D. Bertram, *Annual review of fluid mechanics* **50**, 459 (2018).
  - [4] J. B. Carr, J. H. Thomas, J. Liu, and J. K. Shang, *Journal of Fluid Mechanics* **917**, A10 (2021).
  - [5] H. Mestre, J. Tithof, T. Du, W. Song, W. Peng, A. M. Sweeney, G. Olveda, J. H. Thomas, M. Nedergaard, and D. H. Kelley, *Nature Communications* **9** (2018).
  - [6] J. C. Burns and T. Parkes, *Journal of Fluid Mechanics* **29**, 731–743 (1967).
  - [7] A. H. Shapiro, M. Y. Jaffrin, and S. L. Weinberg, *Journal of Fluid Mechanics* **37**, 799 (1969).
  - [8] A. Farina, L. Fusi, A. Fasano, A. Ceretani, and F. Rosso, *International Journal of Engineering Science* **107**, 1–12 (2016).
  - [9] K. N. Margaritis and R. A. Black, *Journal of The Royal Society Interface* **9**, 601 (2012).
  - [10] N. G. McHale and M. K. Meharg, *The Journal of Physiology* **450**, 503 (1992).
  - [11] D. C. Zawieja, K. L. Davis, R. Schuster, W. M. Hinds, and H. J. Granger, *American Journal of Physiology-Heart and Circulatory Physiology* **264**, H1283 (1993).
  - [12] K. Park, A. Tixier, A. H. Christensen, S. F. Arnbjerg-Nielsen, M. A. Zwieniecki, and K. H. Jensen, *Journal of Fluid Mechanics* **836**, R3 (2018), arXiv:1708.06968.
  - [13] M. Brandenbourger, A. Dangremont, R. Sprik, and C. Coulais, *Physical Review Fluids* **5**, 1 (2020).

Symbol	Description
$R_0$	Radius of the pipe when no external forces are present
$x_v^i$	Position of the $i^{\text{th}}$ valve
$x_v$	Mean valve spacing
$\lambda$	Wavelength of peristalsis
$\epsilon$	$x_v/\lambda$
$n_v$	Number of valves per wavelength = $\epsilon^{-1}$
$\bar{r}_v$	Valve resistance parameter as defined in equation (13)
$\eta$	Strength of peristalsis as defined in equation (9)
$\omega$	Frequency of peristalsis
$\tau$	Elastic relaxation time of the pipe as defined in equation (9)
$\bar{\tau}$	$\tau[1 + n_v \bar{r}_v]$
$\alpha$	Strength of bend
$P_{\text{ext}}$	External radial force per unit area imposed on the tube
$P_a$	Characteristic amplitude of peristalsis
$\bar{x}$	Dimensionless axial length used to study fluid dynamics at large length scales $x/\lambda$
$\bar{y}$	Dimensionless axial length used to study the region between closely spaced valves $x/\epsilon$
$\bar{t}$	Dimensionless time $\omega t/2\pi$
$\xi$	Wave coordinate $\bar{x} - \bar{t}$
$f(x, t)$	Dimensionless peristaltic force $P_{\text{ext}}/P_a$
$P, Q, R$	Fluid pressure, volumetric flow rate, and tube radius
$\bar{P}, \bar{Q}, \bar{R}$	Dimensionless pressure, flow, and radius, as defined by equations (7)
$\bar{\bar{Q}}$	$[1 + n_v \bar{r}_v] \bar{Q}$
$\langle Q \rangle$	Angle brackets denote an average over one period
$P_i$	Subscript $i$ denotes the $i^{\text{th}}$ term in an expansion in powers of a small parameter ( $\epsilon$ or $\eta$ )
$P^O$	Superscript O denotes the solution for an open region of valves in the valve continuum.
$P^C$	Superscript C denotes the solution for a closed region of valves in the valve continuum.
$\tilde{\xi}$	Coordinate at which the valve closes.
$n_v^*$	The value of $n_v$ which maximizes the mean flow.

TABLE II. Parameters used in the paper.

- [14] D. Takagi and N. Balmforth, *Journal of Fluid Mechanics* **672**, 196 (2011).
- [15] S. B. Elbaz and A. D. Gat, *Journal of Fluid Mechanics* **758**, 221 (2014).
- [16] S. Timoshenko and S. Woinowsky-Krieger, *Theory of Plates and Shells* (McGraw-Hill, 1959).
- [17] K. T. Wolf, J. B. Dixon, and A. Alexeev, *Journal of Fluid Mechanics* **918**, A28 (2021).
- [18] M. H. Holmes, *Introduction to perturbation methods*, 2nd ed. (Springer, 2013).
- [19] A. M. Venugopal, C. M. Quick, G. A. Laine, and R. H. Stewart, *American Journal of Physiology - Heart and Circulatory Physiology* **296**, 303 (2009).
- [20] J. B. Dixon, S. T. Greiner, A. A. Gashev, G. L. Cote, J. E. Moore, and D. C. Zawieja, *Microcirculation* **13**, 597 (2006).
- [21] M. Ballard, K. T. Wolf, Z. Nepiyushchikh, J. B. Dixon, and A. Alexeev, *Biomechanics and Modeling in Mechanobiology* **17**, 1343 (2018).
- [22] C. Bertram, C. Macaskill, and J. Moore, *Computer Methods in Biomechanics and Biomedical Engineering* **17**, 1519 (2014).
- [23] T. Ohhashi, T. Azuma, and M. Sakaguchi, *American Journal of Physiology-Heart and Circulatory Physiology* **239**, H88 (1980).
- [24] A. J. Macdonald, K. P. Arkill, G. R. Tabor, N. G. McHale, and C. P. Winlove, *American Journal of Physiology-Heart and Circulatory Physiology* **295**, H305 (2008).
- [25] D. C. Zawieja, *Lymphatic Research and Biology* **7**, 87 (2009).
- [26] J. Alvarado, J. Comtet, E. de Langre, and A. E. Hosoi, *Nature Physics* **13**, 1014 (2017).
- [27] A. Gopinath and L. Mahadevan, *Proceedings of the Royal Society A: Mathematical, Physical and Engineering Sciences* **467**, 1665 (2011).